DECEMBER 2011

Synthesis and Structural Characterization of Metal-Doped Titanate Nanotubes Using TEM, XRD and XAS

Muhammad Yasir

Master's Thesis

FYS M31, 30 hp

Supervisor

Sophie Canton

Research Associate
Department of Synchrotron Instrumentation
Lund University Sweden

To my Parents

Abstract

This work presents the synthesis and structural characterization of titanate nanoproducts, focusing on the effect induced by the presence of silver ion in different concentrations. The synthesis and chemical analysis using TEM, XRD and EDX were performed at the University of Szeged in Hungary. The XAS analysis was done at the MaxLab synchrotron facility in Lund University, Sweden. From the analysis, it is revealed that the titanate nanotubes exhibited an elongated structure before thermal treatment and were transformed into nanocrystals upon thermal treatment at 600 ^{o}C. Silver significantly promoted the conversion of titanate nanotubes into anatase phase, with the participation of new intermediates.

TABLE OF CONTENTS

1. Introduction

1.1 Objectives

Several areas of Nanotechnology focus on the discovery of new materials with unique properties that could lead to improved performances in functioning devices. A large effort is directed worldwide towards the rational design of materials where structure and function are directly coupled. Controlling the shape of nano objects is very important if they are to be used as building blocks in more complex assemblies. The one-dimensonal (1D) morphology encompasses nanoribbons, nanotubes, nanowires, and nanowiskers. It has demonstrated great advantages associated to a unidirectional charge transport in electronics and solar energy applications. In addition, the very large surface to volume ratio with well-defined inner, outer and interstitial regions make these elongated structures highly performant in catalysis.

The discovery of carbon nanotubes has indeed delivered materials with properties distinct from other forms of carbon, such as graphite of fullerenes. Research has since then been extended to other compounds, including semiconductors. Among them, TiO_2 that exhibits a band gap of $\approx$ 3 eV is intensively investigated in connection to biomedical and photoelectrochemical applications. In 1998, Kasuga et al [1] reported a breakthrough protocol for a simple and cheap synthesis of titanate nanotubes, known as the hydrothermal method. It consists of treating TiO_2 precursors with a concentrated aqueous solution of NaOH, thorough HCl washing, followed by heating at moderate temperatures. Very early on, it was recognized that varying the type of the TiO_2 precursors, the reagent concentrations, the overall pH, the washing steps, the heating temperature and time, yield a wide variety of products. Numerous studies have since then been aiming at optimizing the outcome of the hydrothermal method further. One of the main difficulties faced by researchers is the poor monodispersity and crystallinity of the nanotubes. Therefore, obtaining a precise structural description necessitates employing a combination of analytical techniques, including microscopy and X-ray techniques that can provide information on the atomic scale. Transmission electron microscopy (TEM) can be used to record high-resolution pictures of the reaction products (tubular structure, small crystallites …). Energy dispersive X-ray spectroscopy (EDX) provides chemical characterization. X-ray diffraction (XRD) is sensitive to the long range order in a sample. The measured diffraction patterns contain peaks at

different angles, which can be indexed to describe the crystal structure. X-ray absorption spectroscopy (XAS) probes the short range order around a given absorbing atom, including its electronic and geometric structure.

Over the past years, significant improvement has been achieved so that very high quality nanotubes can now be routinely produced and incorporated in practical applications. Their layered structure renders them amenable to the very general ion exchange reaction, where the Na+ and/or H+ ions embedded in the titanate can be replaced by active ions, for example transition metals, imparting enhanced optical and magnetic properties. To date, several issues concerning the details of ion exchanged TiO_2 nanotubes structures as well as the formation mechanisms at play remain nevertheless unresolved.

This work reports the synthesis and characterization through microscopy, EDX, XRD and XAS of silver-doped titanate nanotubes, where the noble metal concentration was varied as a parameter. Comparing the results obtained before and after thermal treatment demonstrates that silver ions play a crucial role in the formation of novel titanate and titania nanostructures that should have great potential for novel practical applications.

2. TiO_2 and TiO_2 Derived Nanotubes

2.1 Significance of TiO_2 and TiO_2 Nanotubes

Titanium is the seventh most abundant metal present in the Earth's crust. It has a very high melting point, a very light weight and is therefore extremely useful in many industrial applications such as aerospace and rocket jet. Titanium Oxide (TiO_2) is a wide band gap semiconductor. It is naturally found in three crystalline forms namely (a) Anatase (I41/amd), (b) Rutile (P42/mnm) and (c) Brookite (Pbca), the first two being the most abundant. The crystal structures are shown in the *Fig. 1*. They consist of chains of TiO_6, where each Ti^{+4} ion is surrounded by six O^{+2} ions forming an octahedron with eight triangular phases and six vertices. The anatase and rutile phases can be differentiated by the degree of distortion from perfect orthorhombic symmetry [2]: it is more important in the former than in the latter. Nanocrystallites of TiO_2 are referred to as titania.

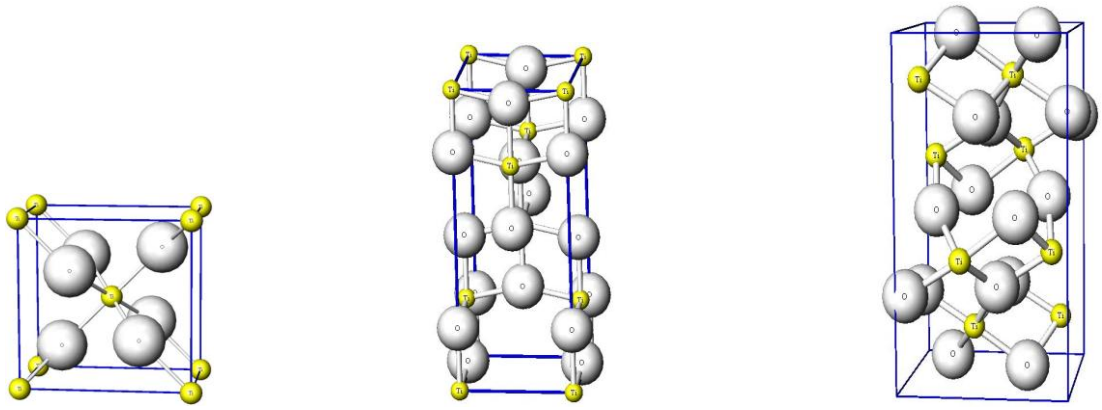

(a)Rutile. (b) Anatase. (c) Brookite.

Figure 1: *Crystal structures of TiO_2 (a) Rutile form. (b) Anatase form. (c) Brookite form.* (*http://www.geocities.jp/ohba_lab_ob_page/structure6.html)*

Importance of the TiO_2 Nanotubular Structure

TiO_2 exhibits remarkable physical and chemical attributes at low cost, such as ultraviolet absorption, stability and catalytic activity. Scientists have tried very early on to build regular nanotubes based this material in order to combined these properties with the advantages of low dimensionality morphology and nanoporosity. It has demonstrated great advantages associated to a unidirectional charge transport in electronics and solar energy applications. The specific surface area of TiO_2 nanotubes can reach 400 $m^2.g^{-1}$ In addition, the very large surface to volume ratio with well-defined inner, outer and interstitial regions make these elongated structures highly performant in catalysis.

2.2. Different Methods used for Synthesis of TiO_2 Nanotubes

Various methods have been proposed for the synthesis of TiO_2 nanotubes, including chemical vapor deposition, templating, sol-gel processes, (Ohsaka, Macak, Fotou, Sato) electrochemical anodizing of titanium metal and the ground breaking hydrothermal synthesis. The last two as described below.

Electrochemical Anodizing

This synthesis method was initially devised to produce aluminum oxide nanotubes. It was later on adapted by Gong et al [3] to TiO_2 nanotubes. Hydrofluoric acid was employed as electrolyte to perform the electrochemical oxidation of titanium sheets, yielding arrays of length up to 500 nm [3] with good control on of pore size. This method is very cost effective to achieve large scale coverage [3].

Hydrothermal Synthesis

This synthesis was first introduced by Kasuga et al. in 1998. A solution of TiO_2 is treated with 10 M NaOH, and heated at 110 ^{0}C for 20 hours [4]. The sample is then washed with HCl and distilled water. Nanotubular structures of length of 100 nm to 200 nm are formed during this process. This simple and cheap reaction only requires a few steps without the need for special chemicals or expensive lab equipment.

Functionalization:

Further functionality, in particular towards light, can be achieved when the TiO_2 nanotubes take part to more complex surface chemistry as reagents or individual building blocks.

Sensitization:

This class of surface modifications includes the adsorption of independent chemical species, ranging from simple functional groups (Shi) to complex macromolecules.

Metal doping/loading:

This class of reaction comprises the surface deposition or volume loading of metal-based species, ranging from simple ions to nanoparticles (bavykin4, zhu2).

Ion exchange:

The so-called ion exchange reaction is a very general chemical method that allows replacing some of the charged species originally present within a solid layered structure by other ones that have different properties. The final product is stable, and reversibility is often observed. This reaction is use in this thesis work with silver ions Ag^+, which is a noble metal with catalytic activity.

2.4. Applications of TiO_2 Nanotubes

TiO_2 has to date found numerous applications thanks to the combined physicochemical properties discussed above.

Photoactivity:

Unlike the rest of the reported titanate materials, the TiO_2 nanotudes are photoacative. At room temperature, they exhibit a photoluminescence spectrum around 400 nm when excited at 236 nm (kudo). This property offers numerous perspectives for optoelectronics applications.

Photocatalitic activity:

TiO_2 nanotubes can take part to photocatalytic reactions. In these processes, an electron gets excited by absorbing a photon having sufficient energy to overcome the band gap (3.03 eV

for TiO_2). This electronic transition from the valence to the conduction band and electron- creates electron-hole pairs and free charge carriers that migrate to the surface. As noted above, an extended photoresponse can also be realized through sensitization so that the full extent of the UV-visible spectral range can be covered in photocatalytic applications. For example, TiO_2 nanotubes have been used as mesoporous catalytic supports for different nanoparticles : CdS-decorated TiO_2 nanotubes are very efficient for dye oxidation (Xiao). Ru(III) hydrated oxide deposited on TiO_2 nanotubes promotes the selective oxidation of alcohols (bavykin). A more than two fold increase in the maximum photoconversion efficiency of water splitting has been observed by replacing TiO_2 nanocrytals by TiO_2 nanowires (zhang2). The rate of water decontamination reactions occur faster if Ag^+ is added to TiO_2 nanotubes (Prasad).

Biomedical Applications:

Several groups have demonstrated the great potential of TiO_2 nanotubes in biomedical applications. For example, they can immobilize metalloproteins that work as mediators of oxygen. Efficient electron transfer takes place between the electrode and the biomolecule. This assembly can be used as biosensor for drug delivery. Recent studies have shown that upon adsorption in the pores of TiO_2 nanotube, the melting point of ibuprofen decreases from 78 ^oC to 66 ^oC, thereby approaching the physiological temperatures. This finding could be utilized to control drug delivery in vivo [5].

Lithium Cells:

TiO_2 nanotubes are also a material of choice for electrode material in the lithium batteries. Carbon-based negative electrodes have serious shortcomings, such as electroplating and the loss of charge due to formation of a solid- electrolyte interface that could be reduced when using TiO_2 nanotubes. Moreover, the rate of diffusion of lithium ions which is one of the processes involved in the charging and discharging of lithium cells could be favored in the elongated TiO_2 nanotubes [5].

3. X-ray Absorption Spectroscopy (XAS)

3.1. Introduction to XAS

Electromagnetic waves that have wavelengths in the range of 0.1 Å to 10 Å are known as X-rays. This highly-energetic radiation is a powerful tool for different types of investigations. Many X-ray based techniques are employed in Material Science, such as X-ray diffraction (XRD), X-ray Photoemission Spectroscopy (XPS), X-ray Reflectivity (XRR), X-ray Raman Scattering (XRS), or X-ray Absorption Spectroscopy (XAS). XAS is a versatile method that can probe the local structure of matter. It is helpful for studying the geometrical as well as the electronic structure of the absorbing atom. An X-ray beam with incident intensity I_o that passes through a material of thickness x, is attenuated to intensity I, following a relation analogue to the Beer-Lambert law that is applicable in the optical regime:

$$ln\left(\frac{I_o}{I}\right) = \mu x \qquad (1)$$

In equation (1), μ represents the linear X-ray absorption coefficient of the material. It depends on the type as well as on density ρ. The ratio (μ / ρ) is called mass absorption coefficient. The linear X-ray absorption reflects the strength of the photoelectric effect. When a photon has enough energy, it can induce a transition from a core shell like s (so called K edge) or p (so called L edge) to the ionization continuum. The kinetic energy of the ejected electron is given by *Eq.3*.

$$E - E_o = \frac{\hbar^2 k^2}{2m_e} \qquad (3)$$

Where, E is the energy of incident photon, E_o is the threshold energy, k is the photoelectron momentum and m_e is the mass of electron. This means that absorption edges (i.e. increase in photon absorption probability) are directly related to the binding energies E_o of the electrons in the sample material. The K-edge absorption spectrum of titanium metal is shown in *Fig. 4.*

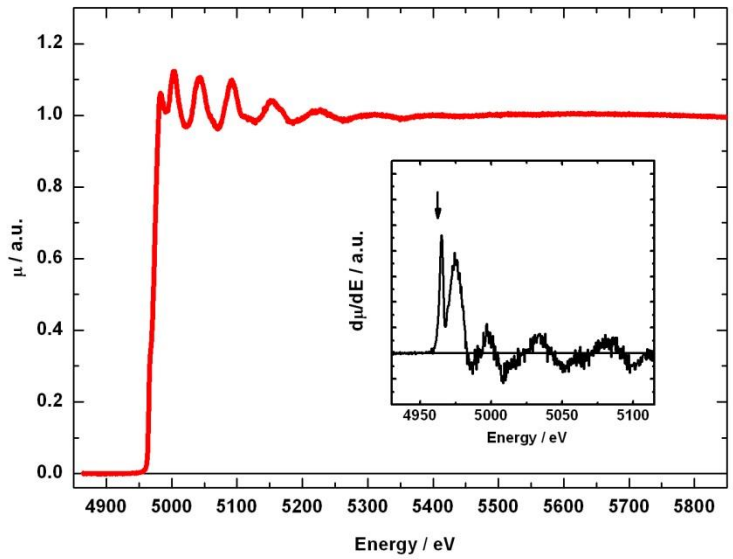

Figure 2: *K - edge XAS spectrum of titanium metal showing E_o at 4.96KeV. [6]*

3.2. X-Ray Absorption Spectra

A typical X-ray absorption spectrum can be divided into four spectral regions: the pre-edge, the XANES, the NEXAFS and the EXAFS regions. A complete spectrum with the corresponding subdivision is shown in *Fig. 3(a).*

Pre-Edge

In the first region, the energy of the incident photons E is less than the absorption threshold E_o ($E < E_o$). The probability of absorption of X-ray is consequently very low. Some very weak features can nevertheless be observed in some instances. They correspond to the electronic transitions from the core level to unfilled energy states within the atom like: s → p or p→ d. The intensities and possible splittings of these spectral lines are very accurate fingerprints for the valency and the coordination geometry of the absorbing atom.

The next three regions correspond to the transitions of core electron to continuum energy states. In these region, the kinetic energy of the free electron can be calculated by $E_k = E - E_o$ (eq. 3)

X-ray Absorption Near Edge Structure (XANES)

The X-ray absorption near edge structure (XANES) corresponds to the region where the incident energy of X-ray E is ±10eV about the absorption edge energy E_o ($E = E_o \pm 10$eV). This region consists of a sharp peak known as 'white line' above the absorption edge. It originates from core electron transition to unbound energy states. These energy states are very densely spaced and form a continuum. Because of this continuum of the states, probability of transition of core electrons to these states increased and it results a sudden increase in the absorption of X-ray photons.

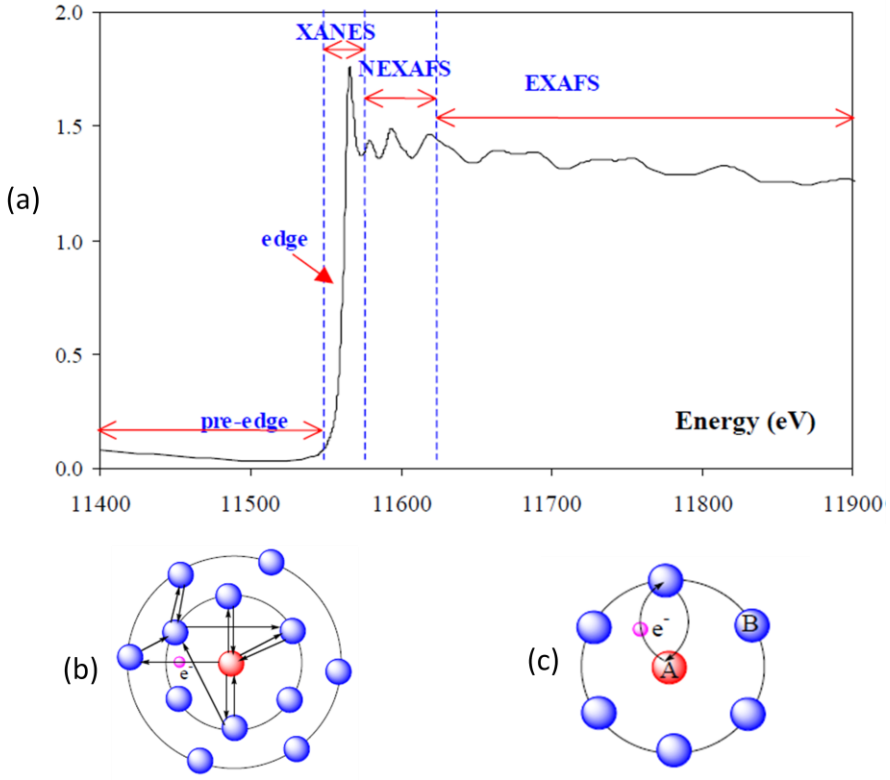

Figure 3: *(a) An X-ray absorption spectrum, showing four different regions. (b) multiple scattering of low kinetic energy photoelectron creates the NEXAFS features. (c) single scattering of ejected photoelectron with high kinetic energy creates the EXAFS features.[6]*

Near edge X-ray Absorption Fine Structure (NEXAFS)

Near edge X-ray absorption fine structure (NEXAFS) encompasses the part of X-ray absorption spectrum where the energy of the incident X-ray E is between 10 eV to 50 eV above the absorption edge. In this region, the ejected photoelectrons have low kinetic energy. Due to their

large de Broglie wavelength, they experience backscattering, not only from the atoms constituting the first shell around the absorbing atom, but also from the further shells, as can be seen in *Fig*. 3(b). These multiple scattering events create modulation features in the NEXAFS region that are very sensitive markers of the local electronic and geometric structure.

Extended X-ray absorption Fine Structure (EXAFS)

Extended x-ray absorption fine structure (EXAFS) is the slowly varying modulation found in the spectral region that starts from 50eV above the absorption edge to beyond. The ejected photoelectrons have high kinetic energy, hence they solely experience single scattering by nearest neighbors around the absorbing atom, as can be seen in *Fig*. 3(c).

3.3. X-ray Absorption Fine Structure (XAFS)

As mentioned above, the XANES and NEXAFS regions are sensitive to the electronic and geometric structure, including valency (oxidation state) and coordination geometry (tetrahedral or octahedral etc), while EXAFS is influenced by the type and number of the surrounding neighbors, as well as their distance from the absorbing atom. The advancement in theory has made it possible to now treat these regions within a unified framework, under the common name X-ray absorption fine structure (XAFS).

3.4. Synchrotron Source for XAS

When a relativistic charged particle (e.g. an electron) accelerates or decelerates, it radiates energy. The wavelength of emitted photons depends on the energy loss of the charged particle. A synchrotron source consists of a ring operating under ultra-high vacuum with curved sections containing magnets that change the path of stored particles. Radio frequency cavities re-accelerate the charged particles after the energy loss. The beam of charged particles is initially injected into the ring kept under ultra-high vacuum. To change the wavelength of radiation, the insertion devices (undulators or wigglers) can be tuned accordingly. Nowadays synchrotron facilities are widely used source of X-ray for many experiments, since they deliver a continuous range of intense X-rays.

3.5. Detection Methods of XAS

Two detection methods are commonly used for recording XAS spectra.

1. Transmission.
2. Fluorescence.

Transmission Method

In this configuration, the collimated X-ray beam passes through the sample. Three ion chambers shown in *Fig*. 3 are used as radiation monitors. The first ion chamber measures the initial intensity I_o. Typically, 20% of the incident beam is absorbed at this step. Following this detector, the sample is mounted perpendicularly to the photon beam. A second ion chamber is located behind the sample to measure the transmitted intensity I_1. The third ion chamber usually absorbs the remaining intensity. A metal foil is placed in front of the third ion chamber for in-line energy calibration purposes. The selection of gases mixture (N_2, Ar and Ne) introduced in all the ion chambers depends on the X-ray energy and the required level of incident absorption.

The transmission method is employed when the concentration of the absorber is high (> 2 wt %). It gives good results for atoms having Z > 16-20.

Fluorescence Method

When an incident X-ray photon ionizes an electron from K or L shells, it creates an inner vacancy. This unstable hole is then filled by an electron cascade from higher-lying shells and fluorescence photons, corresponding to K_α or L_α spectral lines are emitted. Collecting these secondary photons with a Lytle detector constitutes an indirect measurement of the absorption cross section. The sample and the Lytle detector are both oriented at 45^o with respect to the incident beam sample in contrast to the transmission configuration, as shown in *Fig*. 3.

The fluorescence method is used for low concentration of the absorber (< 2 wt %). It gives good results for atoms having Z > 16-20.

Because the reported experiments at the Ti K edge involved X-rays with relatively low energy (4-5 keV), the setup was purged with He gas to avoid excessive absorption by the surrounding ambient air atmosphere.

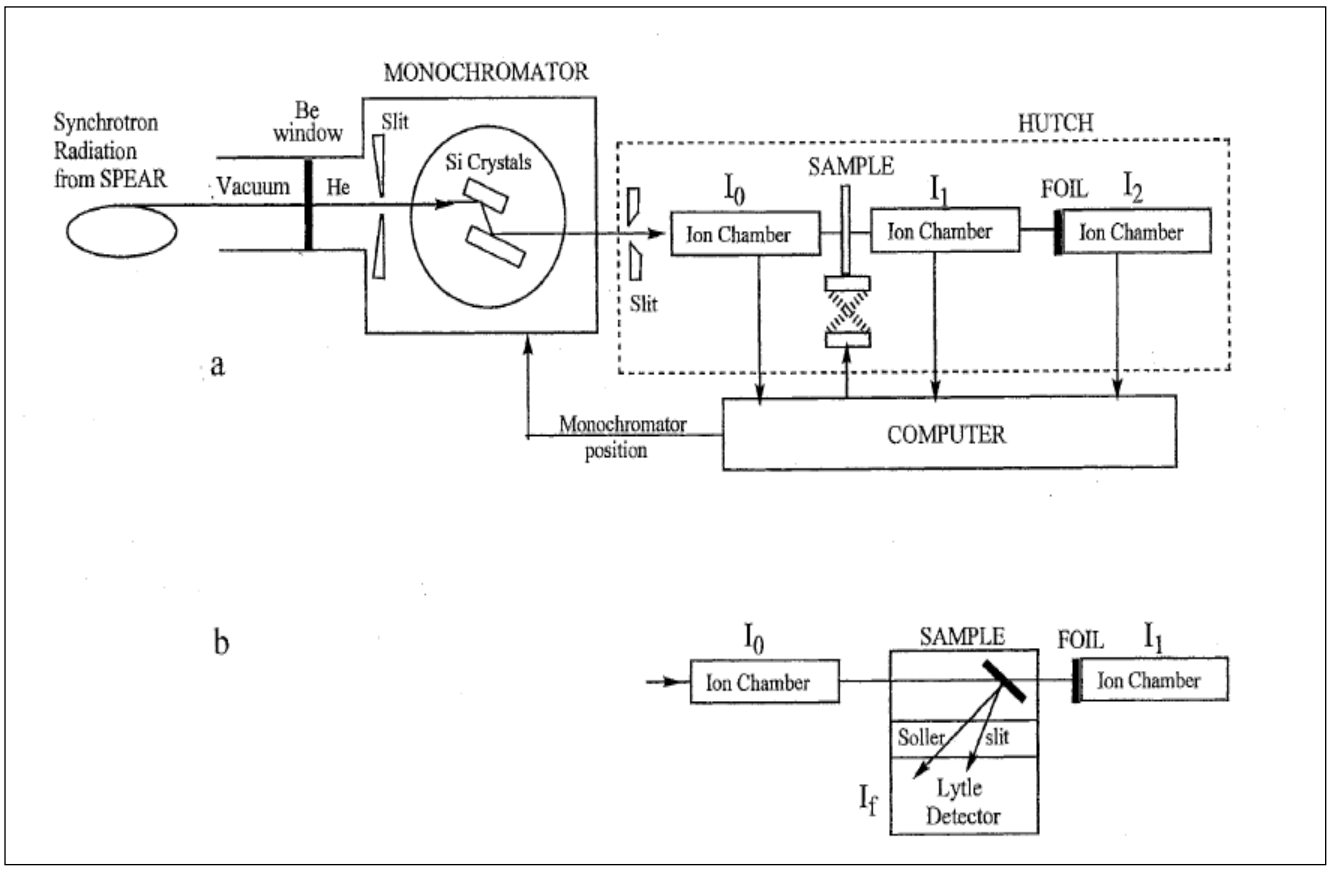

Figure 4: *Experimental setup for XAS measurements (a) The transmission method, showing three ion chambers and the position of the sample. (b) The fluorescence method, showing the placement of sample and Lytle detector.* [6]

4. Transmission Electron Microscopy (TEM)

Transmission electron microscopy (TEM) delivers high-resolution information about the morphology and the structure of a sample, often down to single atoms in favorable cases. In this technique, a beam of energetic electrons is accelerated and transmitted through a thin sample. They are collected and focused onto an imaging device. The resolution is higher than with conventional optical microscopes, owing to the small de Broglie wavelength of the electrons. The TEM images in these experiments were taken with "Philips CM-10 Transmission Electron Microscope".

5. Energy Dispersive X-ray Spectroscopy (EDX)

Energy dispersive X-ray (EDX) spectroscopy is a technique used to identify the elemental composition of a compound. It is an integrated part of a scanning electron microscope (SEM). In this technique, the sample is there also bombarded by an energetic electron beam. Collisions have a high probability to knock out the inner-shell electrons of the constituent atoms. The created vacancy is rapidly filled by an electron from higher lying shell and this transition results in the secondary emission of fluorescence X-rays. Their wavelengths depend on the energy difference between the two shells involved in the electronic transition so that the energy of emitted X-rays is uniquely characteristic of a particular element. In other words, the elemental composition is directly determined by measuring the energy of emitted X-ray. In these experiments, the instrument was a "Hitachi S4700 SEM with Rontec EDS" analyzer.

6. X-ray Diffraction (XRD)

X-ray diffraction (XRD) is employed to determine the crystallographic structure of a sample. The experiments were conducted with a "Rigaku Miniflex II" with a CuKa X-ray, where λ=1.54Å, since the X-rays wavelength is comparable to the interatomic distance, the incident beam is diffracted as it passes through the crystal planes, which are labeled by Miller indices (*hkl*). The diffraction pattern is recorded on a CCD detector. It consists in a set of peaks at different angles. These peaks are used to study determine the crystal structure of the sample.

Each peak in the spectrum of anatase TiO_2 is due to the diffraction of X-ray from any specific plane and it is calculated by comparing analytical and numerical value of distance *d* between two

planes. The directions of plane are represented by miller indices (*hkl*). Bragg's equation $n\lambda=2dsin\theta$ is used for analytical calculation of d where λ represents the X-ray wavelength.

7. Experimental Setup

7.1. Introduction to Beamline I811

The beamline l811 has been constructed at a port of the Max II ring in Max-Lab synchrotron facility. This beamline is dedicated to research studies in Material Science, especially XAS and XRD experiments. The photon energy range delivered at this beamline covers 2.4keV to 20keV [7], corresponding to a wavelength range from 0.6 Å to 5Å [7].

A superconducting wiggler is used as a light source at I811. This insertion device is actually an array of intense magnets, which are used to produce synchrotron radiation by periodically deflecting the beam of charged particles stored in a synchrotron ring [8]. This wiggler has 49 poles, covering a length of about 1.5m. It produces an overall magnetic field of 3.5T.

Optical Design of Beamline I811

The optical layout of l811 shown in *Fig. 5* comprises a combination of collimating and focusing mirrors, as well as a double-crystal monochromator.

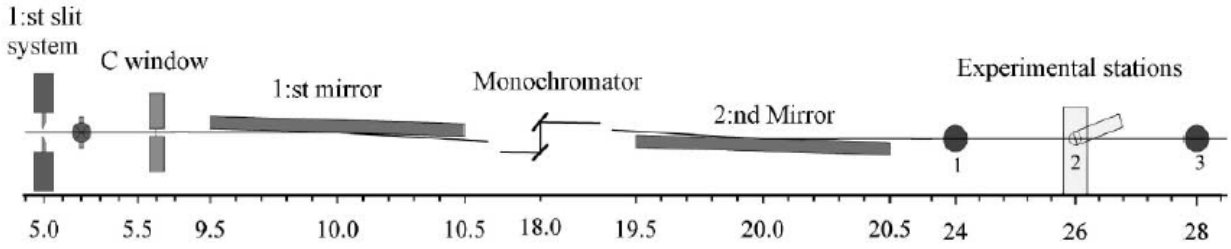

Figure 5: *Simple optical layout of beamline l811 [9].*

The light from the wiggler is reflected and focused by the first mirror onto the monochromator, which selects a narrow range of wavelengths. This double-crystal monochromator consists of two Silicon single crystals. Both of these Silicon crystals can be oriented and positioned very precisely in the X-ray beam. The *Si* (*111*) reflection is used for experiments requiring a low incident energy, while the *Si* (*311*) is used for obtaining high energies. From this point on, the photons are quasi monochromatic. The beam is further focused in the experimental station the second mirror. The photon flux on the sample is about 10^{11} - 10^{12} ph/sec at 9keV [7].

8. Programs Used for XAS Simulation

8.1. ATOMS Program

The analysis of a XAS spectrum relies on a structural model, which can be built once the positions of the atoms with respect to the absorbing element are known. The 'ATOMS' program delivers the set atomic coordinates (XYZ) from the measured set of crystallographic parameters. The web application of the program ATOMS called WebATOMS was used in the following section.

The crystallographic parameters contain information about the unit cell and the atomic positions in factional coordinates (x,y,z). The unit cell can be seen as the basic building block that repeats periodically throughout the crystal. It is defined by lattice parameters shown in *Fig. 6*, which included three distances (denoted by a, b and c) called lattice constant and three angles (α, β, γ) between these sides called lattice angles.

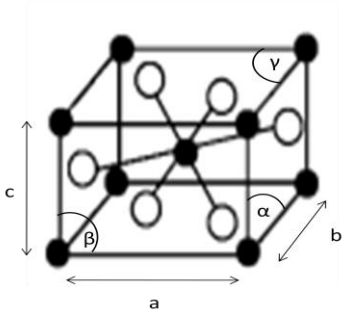

Figure 6: *TiO_2 crystal structure with lattice constants (a, b, c) and lattice angles (α, β, γ). Black and white circles represent Ti and O atoms respectively.*

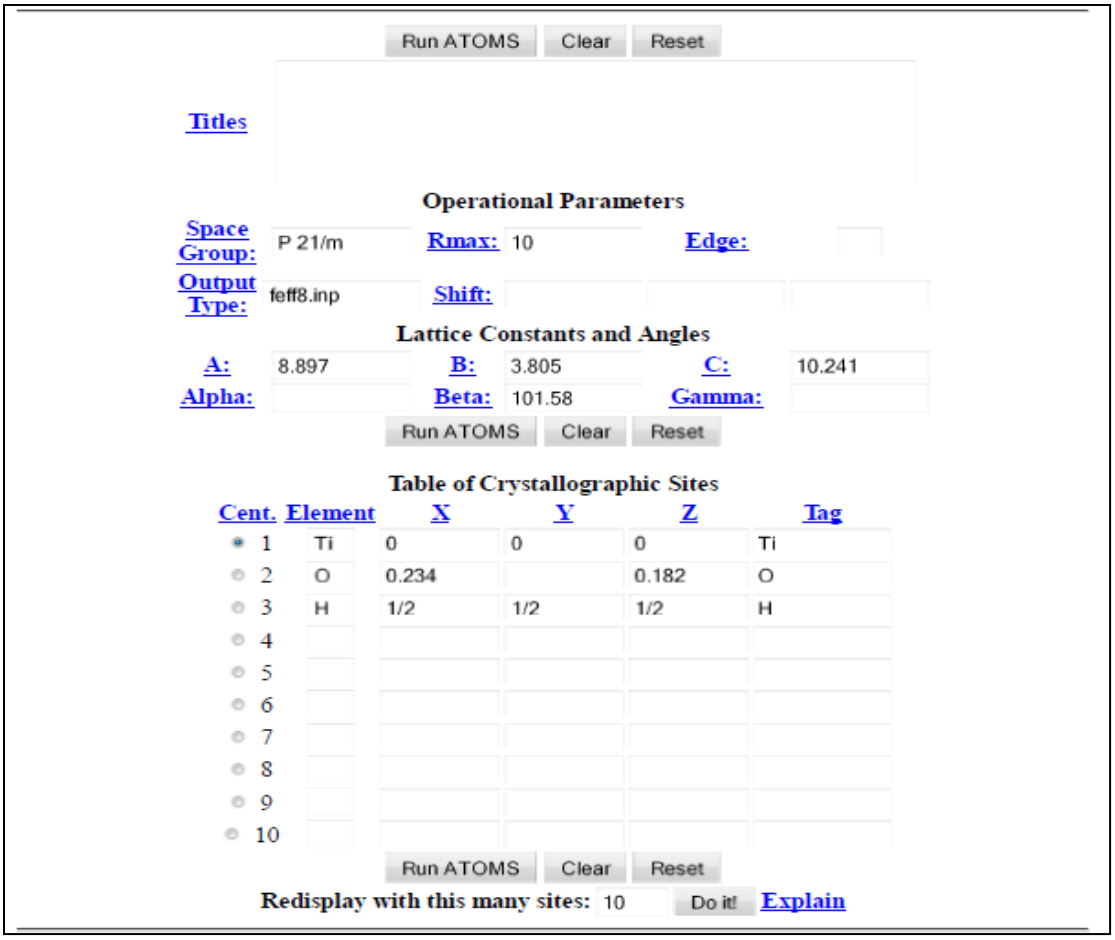

(a)

```
POTENTIALS
*    ipot    Z   element            l_scmt  l_fms    stoichiometry
       0    22    Ti                  2       2        0.001
       1    22    Ti                  2       2        2
       2     8    O                   1       1        4
       3     1    H                   1       1        2

ATOMS                              * this list contains 105 atoms
*    x          y          z       ipot  tag           distance
    0.00000    0.00000    0.00000  0     Ti            0.00000     0
    0.00000    1.90250    0.00000  1     Ti            1.90250     1
    0.00000   -1.90250    0.00000  1     Ti            1.90250     2
    2.03952    0.00000    1.44595  2     O             2.50008     3
   -2.03952    0.00000   -1.44595  2     O             2.50008     4
    2.03952    1.90250    1.44595  2     O             3.14164     5
    2.03952   -1.90250    1.44595  2     O             3.14164     6
   -2.03952    1.90250   -1.44595  2     O             3.14164     7
   -2.03952   -1.90250   -1.44595  2     O             3.14164     8
    0.00000    3.80500    0.00000  1     Ti            3.80500     9
    0.00000   -3.80500    0.00000  1     Ti            3.80500    10
```

Figure 7: *(a) WebATOMS input and output. (b)The output of (a) showing positions of different atoms by means of (X, Y, Z) coordinates.*

8.2. FEFF Program

The FEFF program is used to model the different XANES and XAFS spectra originating from a given cluster of atoms. This program calculates the XAFS equation (*Eq. 4*) and generates XAFS spectra from the set of (X,Y,Z) coordinates. The XAFS oscillations χ_i (k) can be represented by a sum of modified sine waves that are good approximation for the wave functions of the free photoelectron. The phase of these sine waves are modified when backscattering from the surrounding shells *j* occurs, so that the free electron wave function can now be written as :

$$\chi_i\ (k) = \Sigma_j\ A_j\ (k)\sin[\Psi_{ij}\ (k)] \qquad (4)$$

where A_j represents the backscattering amplitude form j^{th} shell, and Ψ_{ij} (k) the associated phase function. Following the development in Scattering Theory, the formalism was extended to take into account the contribution of multiple scattering. The XAFS equation can be written as

$$\chi_i\ (k) = \Sigma_j\ \frac{N_j . S_o^2(k)}{k . R_j^2} \left| f_{eff}\ (k) \right| . \exp\left(-2k^2\sigma_j^2\right) . \exp\left[\frac{-2R_j}{\Lambda(k)}\right] . \sin\left[2kR_j\ + \phi_{ij}\right] \qquad (5)$$

where N_j is the number of neighboring atoms in j^{th} shell (i.e. the coordination number), R_j is the distance between the central atom and the neighboring atoms in j^{th} shell, $S_o^2(k)$ is the reduction in amplitude due to multiple excitations, f_{eff} (k) is the effective amplitude function for each scattering path, $exp\ (-2k^2\sigma^2_j)$is The Debye-Waller factor, σ_j is the Debye- Waller parameter that accounts for thermal configurationally disorder, Λ (k) is the mean free path of the photoelectron, $exp\ [-2R / \Lambda\ (k)]$ is the mean free path factor, $[2kR_j + \phi_{ij}\ ]$is total phase and ϕ_{ij} is the phase shift because of coulomb potential of central atom *i* as well as back scattering atom *j*.

The feff.inp file contains the information needed for calculating XAFS equation. This information is coded through different keywords called cards. TITLE contains the title line written by the user to identify the specific file. POTENTIALS associates a unique number to a the scattering potential originating from a pair of atoms. The ATOMS card contains the symbol and (X,Y,Z) coordinates of the absorbing and surrounding atoms, which is the case of TiO_2 are Ti and O. POTENTIALS associates a unique number to a the scattering potential originating from a pair of atoms. All distinguishable atoms are assigned a unique potential index which is used to calculate the shift in the phase of wave due to scattering. END is entered when the file is completed.

```
 * This feff.inp file generated by ATOMS, version 2.50
 * ATOMS written by and copyright (c) Bruce Ravel, 1992-1999

 * -- * -- * -- * -- * -- * -- * -- * -- * -- * -- * -- * -- * -- * -- *
-- * -- *
 *       total mu =     1497.9 cm^-1, delta mu =     1277.4
cm^-1
 *       specific gravity =  5.256, cluster contains   90
atoms.
 * -- * -- * -- * -- * -- * -- * -- * -- * -- * -- * -- * -- * -- * -- *
-- * -- *
 *       mcmaster corrections:  0.00065 ang^2 and  0.813E-06
ang^4
 * -- * -- * -- * -- * -- * -- * -- * -- * -- * -- * -- * -- * -- * -- *
-- * -- *

 TITLE   name:     Na2Ti307
 EDGE      K
 S02       1.0

 *         pot    xsph  fms   paths genfmt ff2chi
 CONTROL   1      1     1     1     1      1
 PRINT     1      1     1     1     1      3


 EXAFS
 RPATH     8.56094

 POTENTIALS
 *   ipot   z
       0   22    Ti
       1    8    O
       2   22    Ti
      3   11    Na


 ATOMS
    4.893    0.941    5.541  3     Na
    4.249    0.941    1.434  3     Na
   -0.336    0.941    2.613  0     Ti
    0.813    0.941    6.268  2     Ti
   -0.773    0.941    9.137  2     Ti
    1.581    0.941    1.816  1     O
    0.271    0.941    4.405  1     O
    2.593    0.941    6.007  1     O
    0.975    0.941    8.242  1     O
    7.414    0.941    6.938  1     O
    6.463    0.941    2.915  1     O
    8.078    0.941    0.289  1     O
  END
```

Figure 8: *Example of 'feff.inp' file used to run FEFF program for* $Na_2Ti_3O_7$.

8.3. WinXAS Program

The data obtained from a XAS experiment is analyzed by using the WinXAS program. Corrections in the raw spectra have to be performed first and they are discussed below.

Modification of Abscissa

The program requires an *x* axis in keV. Since the energy value is initially in eV in the experimental data, the abscissa is multiplied by 0.001.

Correction of Pre- Edge Background

The presence of other atoms in the sample causes a background signal before the absorption edge of interest. A linear polynomial fit to the flat spectrum in this region is performed and subtracted from the raw data.

Normalization

In general, the concentration of absorbing atoms in the sample and the exact thickness are unknown. This does affect the height of the edge jump. In order to remove the influence of these parameters, the post-edge amplitude is normalized to unity. This also facilitates the comparison of different samples.

Threshold energy E_o

In this step, the energy scale from keV to wavenumber *k* according to the energy conservation equation (3). The threshold energy E_o is first approximated as the first maximum in the first derivative of the XAS spectrum, and it is one of the fitting parameters used by FEFF.

Removal of Atomic background

The XANES and EXAFS information can be extracted from the analysis the *X (k)* function defined as:

$$X(k) = \frac{[\mu(k) - \mu\_0\ (k)]}{\mu_0(k)}.$$

where, $\mu_0\ (k)$ is the absorption coefficient of the **isolated** atom, while $\mu\ (k)$ is the absorption coefficient of the same atom, but in the particular **sample environment**. In fact, $\mu_o\,(k)$ can never

be measured experimentally. It is usually approximated by a smooth curve $\mu_{spline}(k)$, which is numerically determined through fitting the experimental data over the whole energy range.

Fourier Transform

The XAFS oscillation expressed in *k*-space depends on the phase shifts enforced by the neighboring atomic shells on the wavefunction of the free electron. A Fourier transformation into the real space (r-space) is performed on this XAFS function to get the information about the distances between central absorbing atom and backscatterer. A peak at a particular distance can be interpreted as a large backscattering probability, hence as a neighbor position.

9. Experimental Section

The synthesis of titanate nanowires and nanotubes, the ion exchange with silver ions Ag^+ and the material characterization via TEM, XRD and EDX were performed at the University of Szeged in Hungary. The XAS experiments were done at the MaxLab synchrotron facility of Lund University in Sweden.

9.1. Synthesis of Titanate nanotubes and Titanate nanowires.

The TiO_2 nanoproducts were synthesized through the hydrothermal process. Anatase-type TiO_2 was added to a 10M aqueous solution of NaOH. The solution was placed into a Teflon-lined autoclave, then after into the furnace at 189 ^oC for 24 hours. The furnace had a motor to rotate the autoclave containing TiO_2 suspensions. This rotation was necessary to make the nanowires but was not necessary to produce nanotubes. After 24 hours, filtration was done, with distilled water, then using HCl and once more with distilled water, in order to replace the Na^+ presented by H^+. After filtration, the sample was placed into a dryer at 60 ^oC for 24 hours. The final products were titanate nanotube or titanate nanowire. The titanate nanotubes (TiNT) sample was named G172, while the titanate nanowires (TiNW) sample was named as G173. These products are inorganic compounds that contain titanium oxide and so belong to the titanate family.

Metal Ion Exchange In Titanate Nanotubes:

The base material G172 was used as a starting material. The Na^+ and H^+ ion from G172 were replaced by metal ions following two routes. In first method, Ag with different concentrations was used. In the second one, different metals Fe, Ni, and Co with the same concentration of 20mmol/g were used. Suspensions of titanate nanotubes with water in different jars were prepared. Sonication was performed on the aqueous suspensions of titanate nanotubes to separate them from each other. The Ag^+ was added into the solutions with different concentrations (0.1, 0.2, 0.5, 1, 2, and 5 mmol Ag^+/g-TiNT). Each solution was filtered after 72-hours of stirring and washed separately with distilled water. All samples were placed into a dryer at 60^oC for 24-hours. After drying, the thermal treatment was done at 600^oC for 24-hours.

9.2. Results and Discussion

Morphology (TEM)

Titanate nanowires with and without metal Ion exchange.

TEM was used study the structure of the titanate nanowires with and without metal ion exchange. As seen in *Fig.9 (a),* the initial sample has the wire form. The length of the tubes is about 1.5µm with a diameter of about 60nm on average. The black spots that appeared in *Fig.9 (b)* show the growth of silver metallic nanoparticles that have diameters around 5- 7nm.

(a) 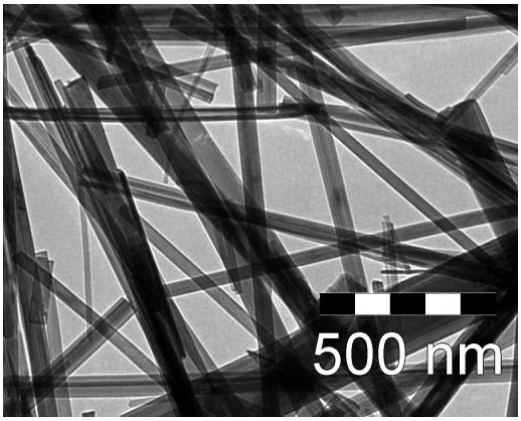

(b) 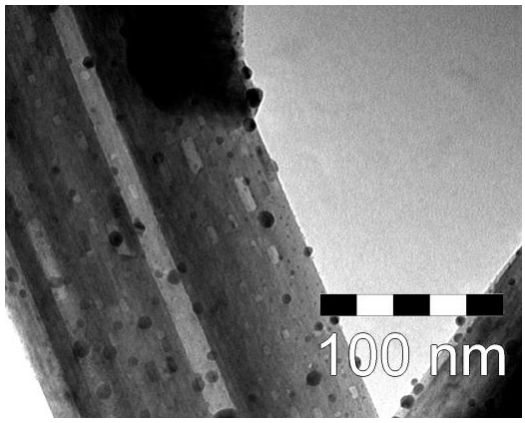

Figure 9: *(a) TEM image of titanate nanowires. (b) TEM image of titanate nanowires with growth of silver (Ag) on the surface.*

Titanate nanotubes with metal ion exchange and different concentrations of metal ions before and after thermal treatment.

Titanate nanotubes with different concentrations of silver ions were studied by using TEM, XRD and EDX. Six samples of titanate nanotubes were considered, with silver concentration of 0.1, 0.2, 0.5, 1, 2 and 5mmol/g. *Fig.10 (a)* shows the TEM image of sample with 0.5mmol/g of silver before thermal treatment. It is clear from the images that the sample has a tubular structure. There is no apparent change in structure before thermal treatment due to the ion exchange. Following this reaction, silver ions are on the surface and within the interlayer spacings. *Fig. 10(b), 11(a)* and 11*(b)* show the thermally treated Ag Titanate nanotubes with 0.5, 0.2 and 2mmol/g respectively. It can be seen that the elongated nanotubular structure of the sample has disappeared and has transformed into plate-like nanoparticle structures. Another finding is the

appearance of Ag particles on structure is less in the 0.2mmol/g and greater in 2mmol/g with an average size of 0.5-1 nm as shown in *Fig. 11(a) and 11(b)* respectively.

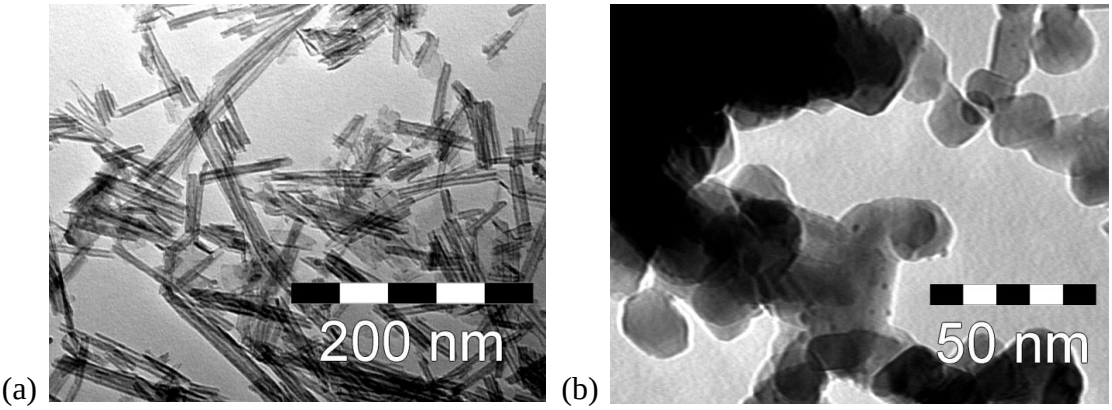

***Figure 10**: TEM images of titanate nanotubes with different concentrations of Ag. (a) 0.5mmol/g Ag without thermal treatment. (b) 0.5mmol/g Ag after thermal treatment.*

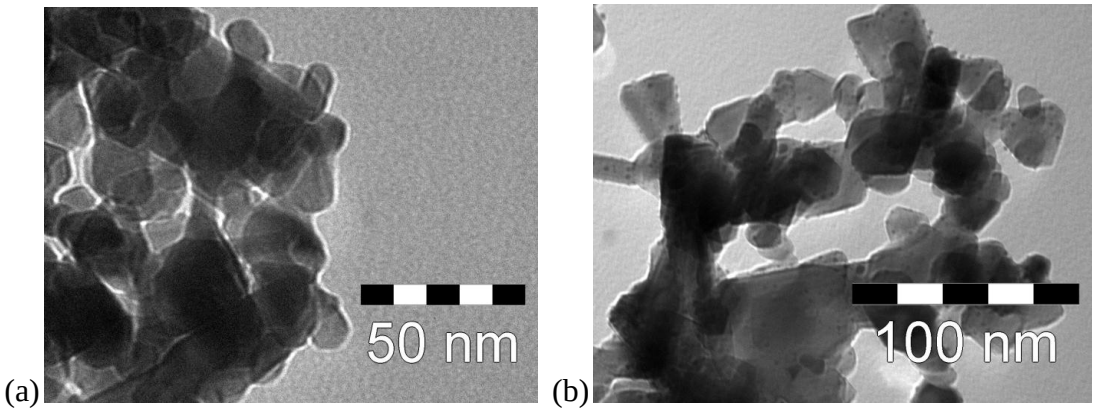

***Figure 11**: TEM images of titanate nanotubes with different concentrations of Ag. (a) 0.2mmol/g Ag after thermal treatment. (b) 2mmol/g Ag after thermal treatment.*

Chemical Analysis (EDX)

Fig. 12 displays the EDX measurements carried out for the elemental analysis of thermally treated silver titanate nanotubes. The concentration of different elements within Ag/TiNT can be seen in EDX spectrum. *Fig.12* shows that the product a has high content of Ti, Ag and O, while Na and Al are also present with lower concentration.

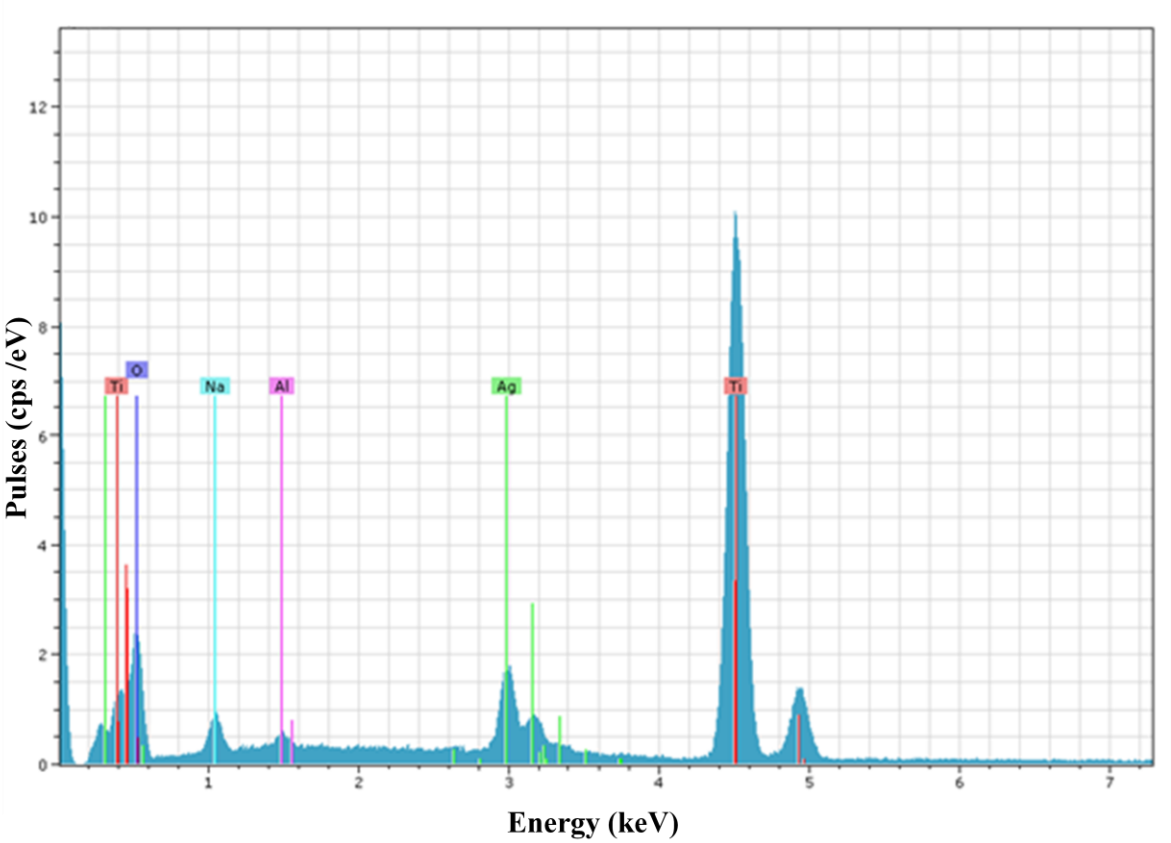

Figure 12: *EDX spectrum of thermally treated Ag/TiNT.*

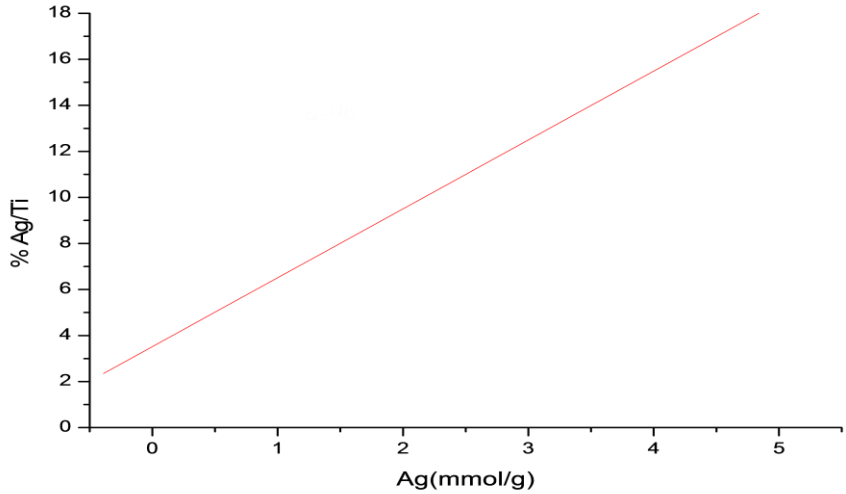

Figure 13: *Concentration of Ag nanoparticles in thermally treated AgTiNT as a function of* $AgNO_3$ concentration.

It can be seen in *Fig. 13* that the concentration of Ag contents increases with increase in the concentration of Ag in the given solution, which is not surprising

X-ray Diffraction

Before thermal treatment

The XRD patterns of silver treated titanate nanotubes in *Fig. 15* were taken before the thermal treatment of samples and *Fig. 16* shows XRD patterns of thermally treated samples. To find the crystal structure of samples at any stage (i.e. before or after thermal treatment), we compare these XRD patterns with standard TiO_2 spectra and base material sample G172 shown in *Fig. 14* and find actual phase of the sample at that stage. After the ion-exchange process the tubular morphology survives at the low silver-ion concentration. At higher concentration the layered structure disappears (reflections around $2\theta = 10^o$ are declined) shown in *Fig. 15*.

Each peak in the spectrum of anatase TiO_2 is due to the diffraction of X-ray from a specific plane. They can be calculated by comparing analytical and numerical value of distance *d* between two planes. The directions of the plane are represented by Miller indices (*hkl*). Bragg's equation $n\lambda=2d\sin\theta$ is used for analytical calculation of *d* where λ represents the wavelength of X-ray. As mentioned above, these experiments used CuKa X-ray source with λ= 1.54Å and θ is the angle of diffraction and it can be measured from the XRD graph. Since the anatase TiO_2 has

tetragonal structure with lattice constant $a = b \neq c$, the numerical value of d for tetragonal structure was calculated using equation

$$d = \left[\frac{h^2 + k^2}{a^2} + \frac{l^2}{c^2}\right]^{-\frac{1}{2}}$$

where *h,k* and l are the Miller indices and $a = 3.74$Å and $c = 9.50$Å are lattice constant discussed in *section 8.1*.

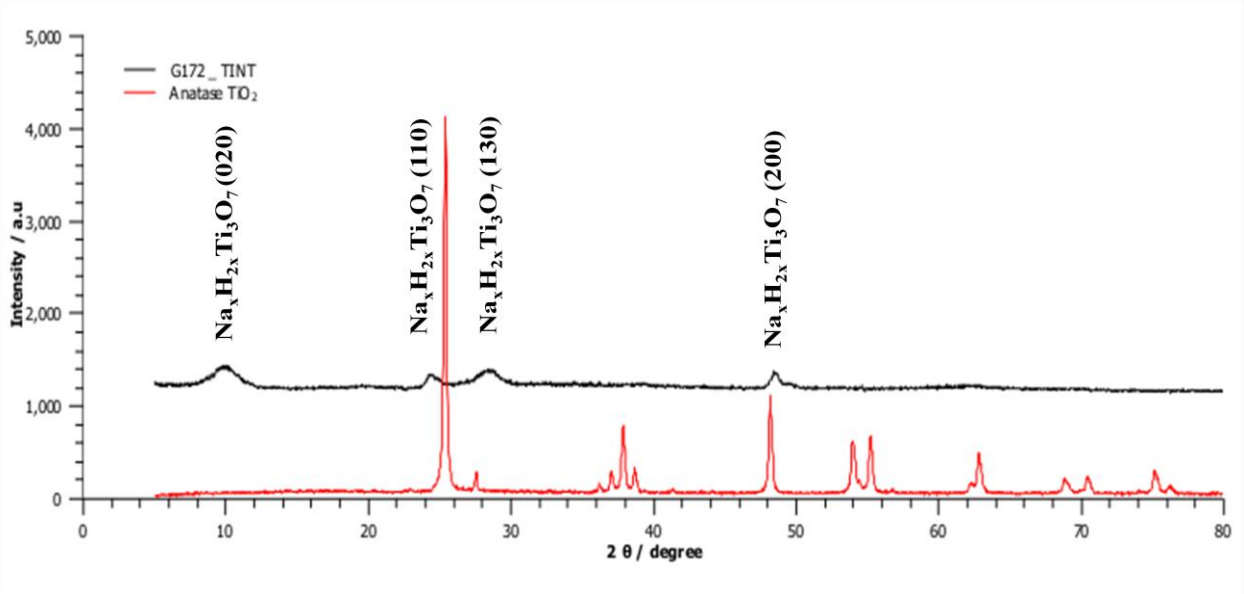

Figure 14: *XRD pattern of base material G172 (titanate nanotubes) and anatase TiO_2*

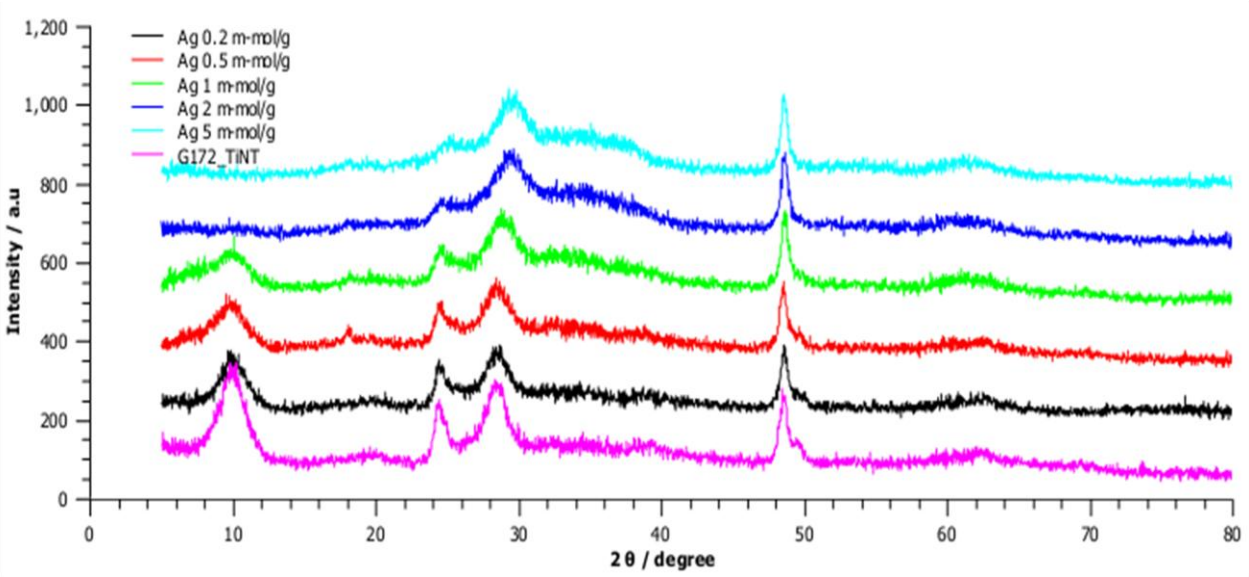

***Figure 15**: XRD pattern of titanate nanotubes with different concentrations of Ag before thermal treatment*

After thermal treatment

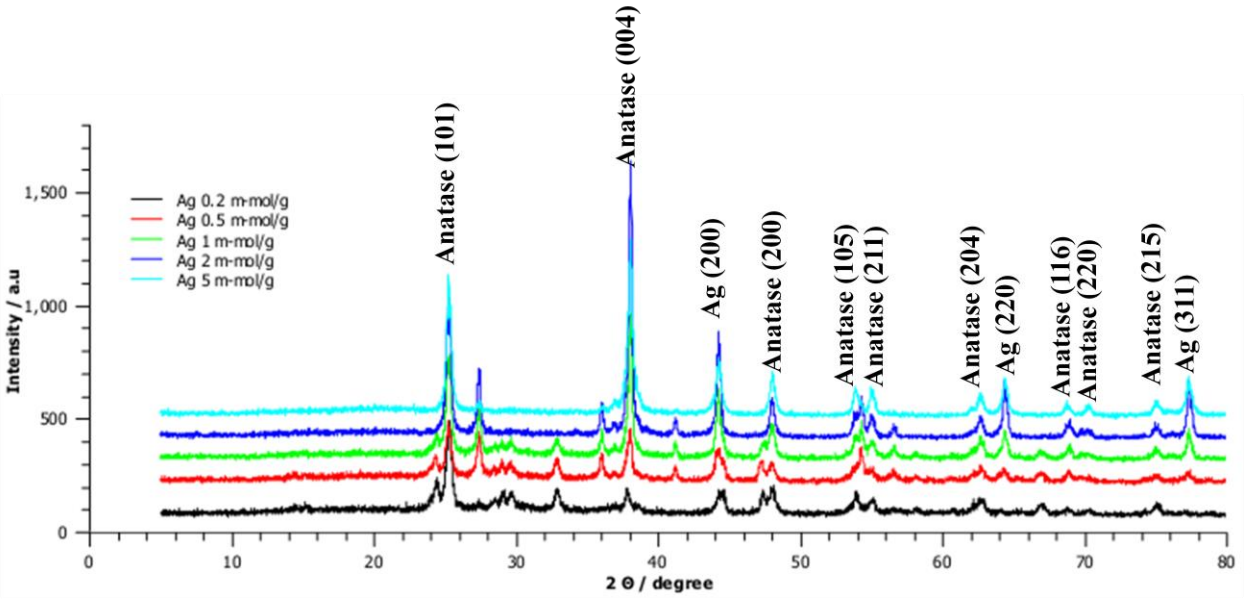

***Figure 16:** XRD pattern of titanate nanotubes with different concentrations of Ag after thermal treatment.*

By comparing the *Fig. 14*, *Fig. 15* and *Fig. 16,* it can be concluded that the reflections of silver containing titanate before thermal treatment are close to the nanotubular base material. Apart from the loss of layered structure at high Ag concentrations, there are no noticeable structural changes in the nanotubular structure. Some of the reflections of thermally treated silver titanate are merged with the ones of TiO_2 in anatase phase, but several new ones are actually observed. This is one of the important findings of this work: the thermal treatment of Ag loaded titanate nanotubes produces new titanate nanoobjects. Their crystallographic assignment is still work in process. As observed in *Fig. 16,* the peak at $2\theta = 38.1^{o}$ is getting more intense than the previous peak at 25^{o} for anatase. This peak is ascribed to the reflection from (111) crystalline plan of metal silver. The reflexes in thermally treated silver titanate are better defined and narrower. This shows that the products have a high crystallinity that increases with the concentration of silver. This is due to the fact that Ag^{+} has high reduction potential. Other characteristic reflections of silver metal crystalline planes can also be seen in the spectrum of thermally treated samples. It is inferred from the XRD spectrum that Ag^{+} ions before thermal treatment have been converted into metallic form upon thermal treatment. They play a crucial role in the appearance of the new titanate structures formed at high temperatures.

X-ray Absorption Spectroscopy

The XAS analysis of the TiO_2 anatase is performed first as reference sample. The XAS spectra of the loaded samples before and after thermal treatment are then compared discussed.

Anatase (reference sample)

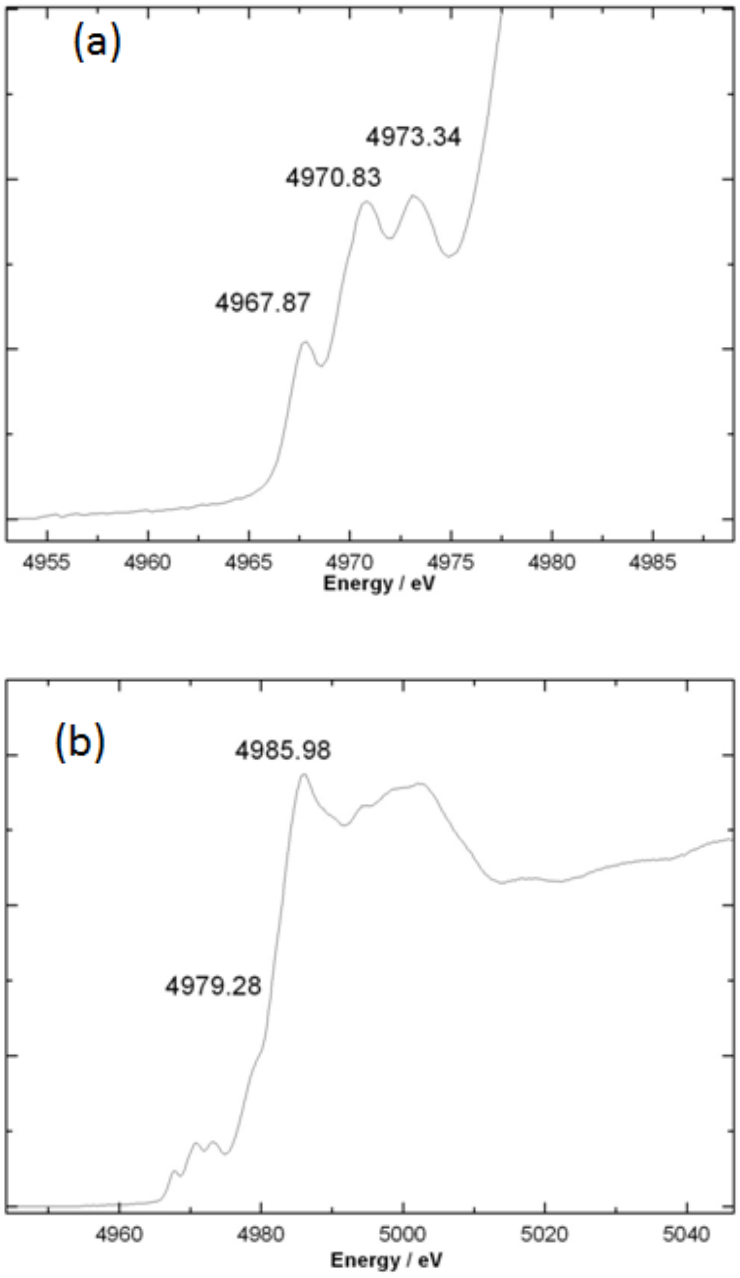

***Figure 17**: XAS spectra of anatase TiO_2 (a) Pre-edge region. (b) XANES spectra.*

Before thermal treatment- Effect of different [Ag^{+}]

Overview

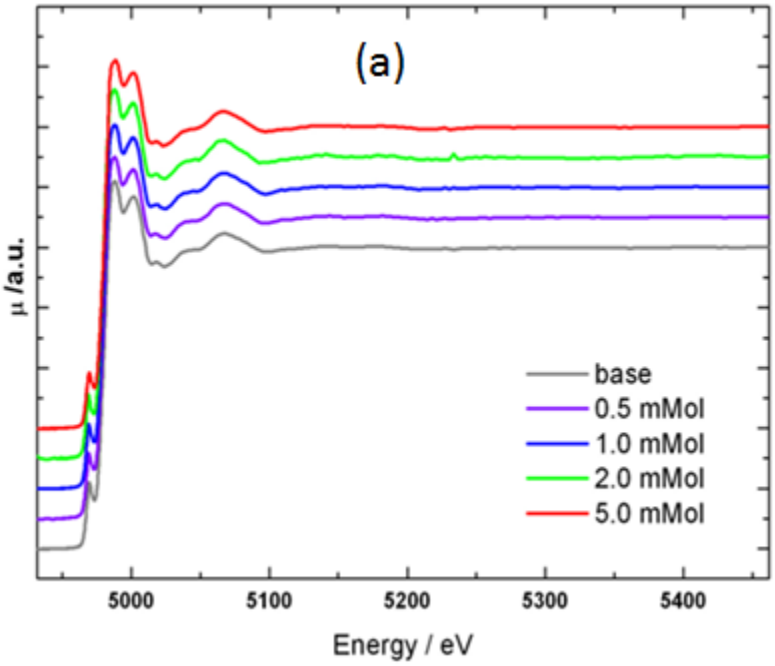

Pre edge

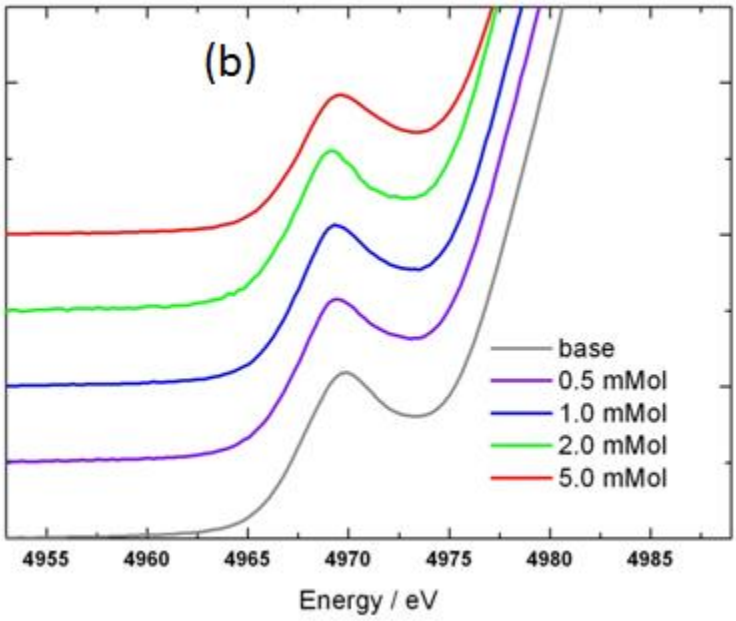

XANES

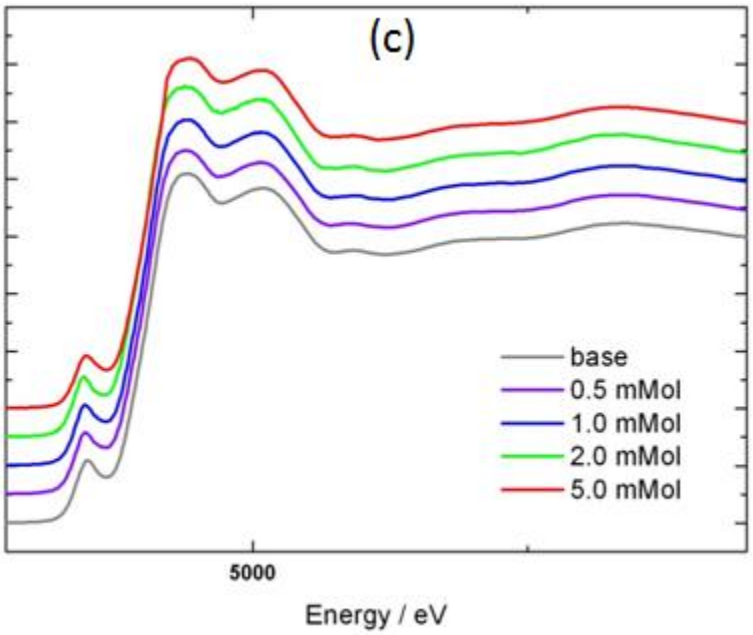

1st Derivative function of XANES spectra

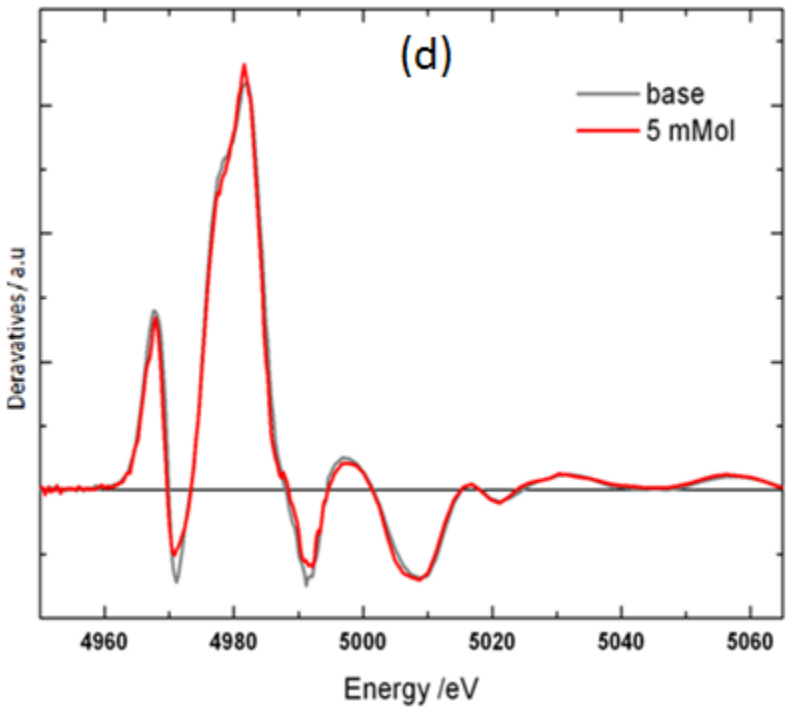

Figure 18*: XAS spectra of sample before thermal treatment having different concentrations of silver (a) Overview of XAS spectrum. (b) Pre-edge region. (c) XANES region. (d) The first-derivative functions of XANES spectra.*

After thermal treatment comparison

Overview

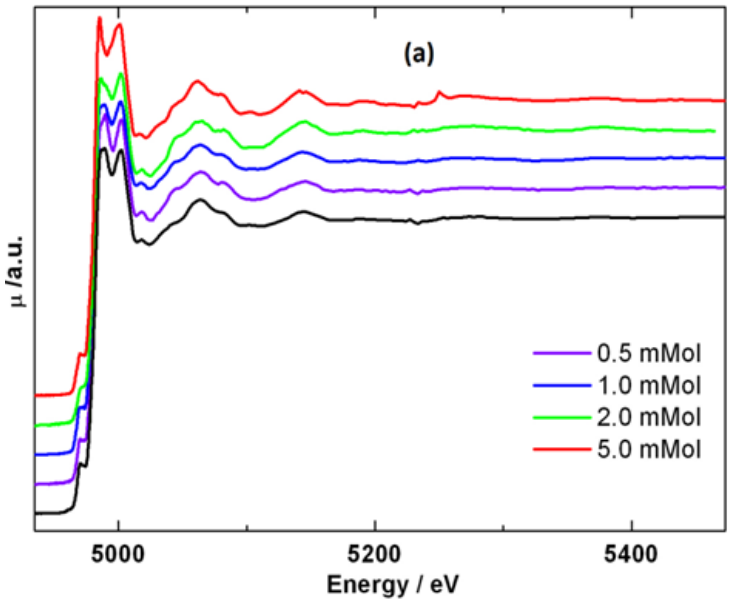

Preedge

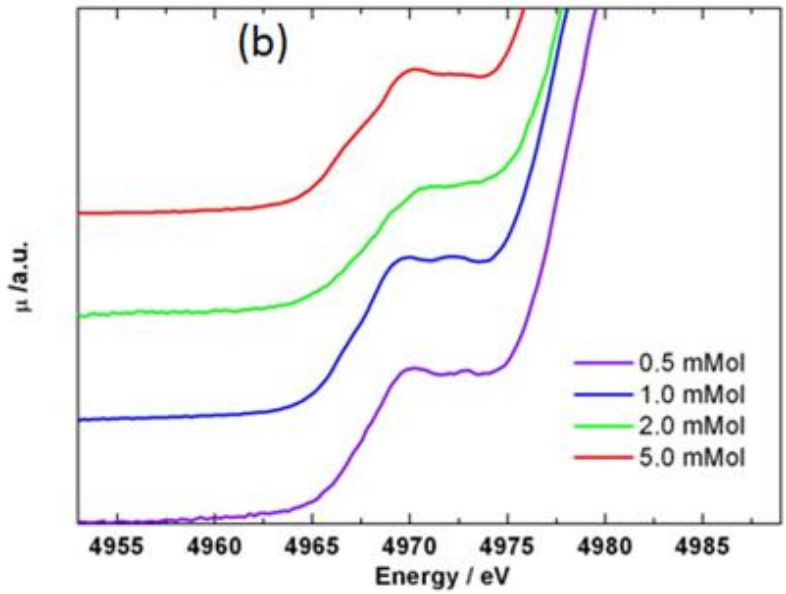

XANES

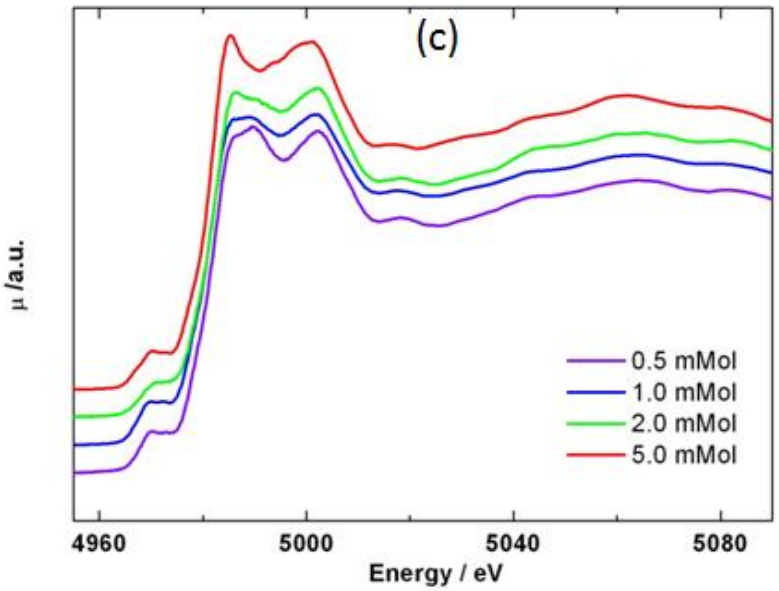

1st Derivative function of XANES spectra

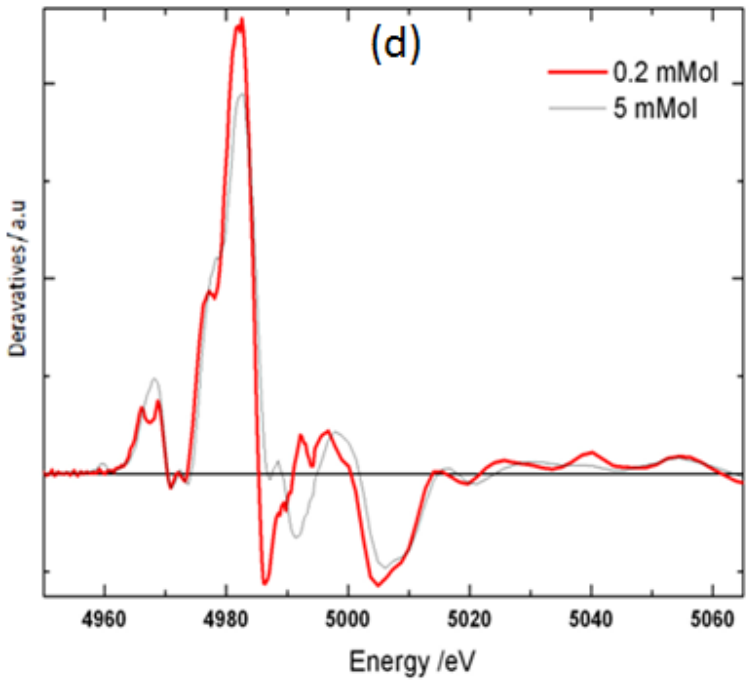

Figure 19*: XAS spectra of sample after thermal treatment having different concentrations of silver (a) Overview of XAS spectrum. (b) Pre-edge region. (c) XANES region. (d) The first-derivative function of XANES spectra.*

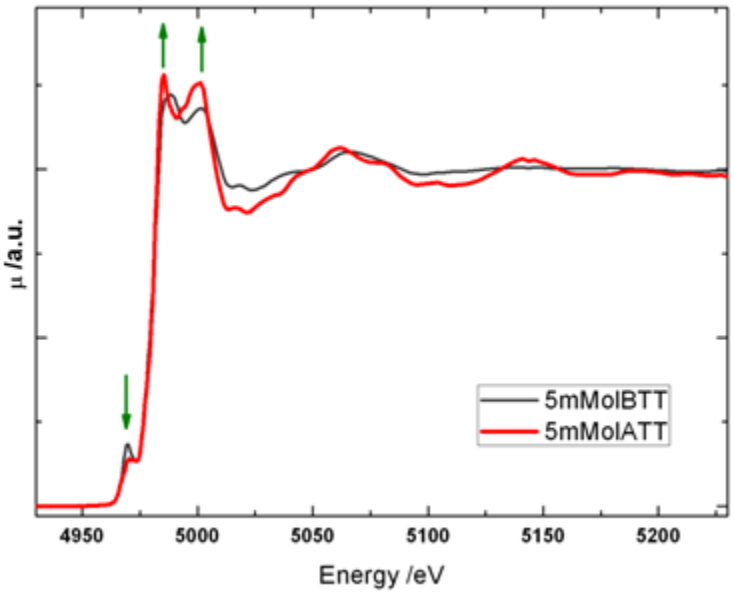

Figure 20: *Comparison between XAS spectrum of 5mmol treated and not treated samples.*

EXAFS and R- distribution

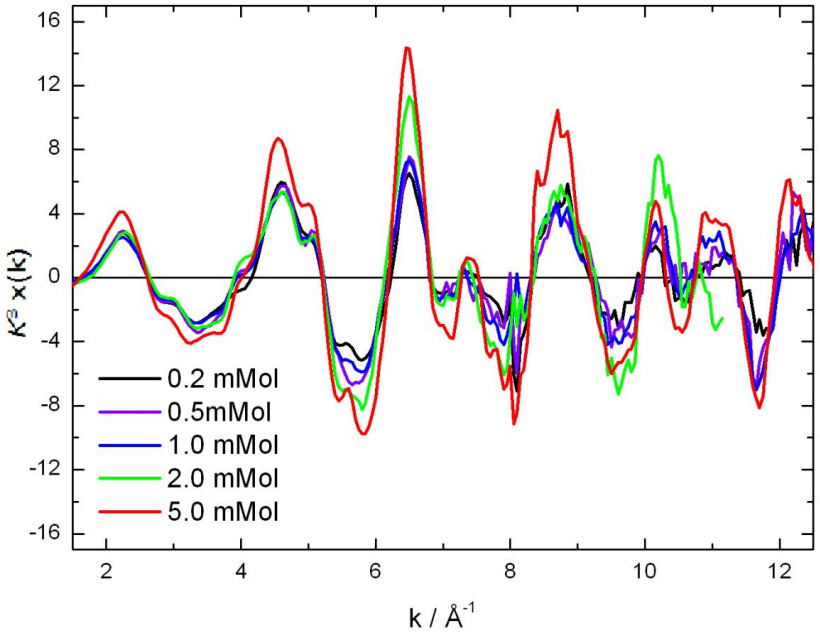

Figure 21: *k^3-weighted EXAFS oscillation for thermally treated silver titanate for different concentrations of Ag.*

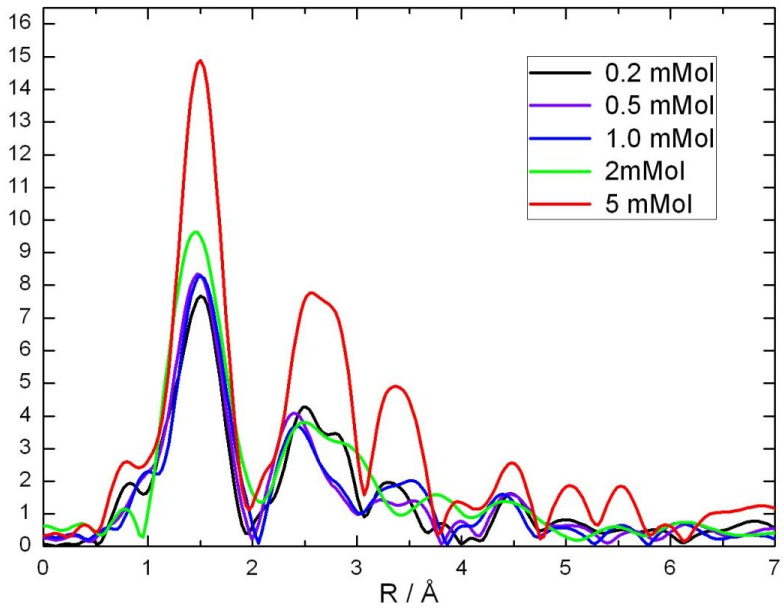

Figure 22: *Fourier Transformed EXAFS of samples contains Ag metals*

After thermal treatment

The pre edge features of TiO_2 in anatase form and treated and not treated silver titanate samples can be seen in *Fig. 17(a)*, *Fig. 18(b)* and *Fig. 19(b)* respectively. The pre edge features of thermally treated samples clearly showed that the peak that was present in non-thermally treated sample is getting lower in the intensity and shifts in energy. This can be associated with the sample transforming again into anatase phase and moving towards octahedral symmetry. The effect of concentration of Ag metal is also clear. The figures all show that with the increase of concentration of silver metal the energy shift is also increased. The most prominent energy shift can be seen in the silver titanate with 5m-mol/gm and it is very close to the energy position in anatase phase.

9.3. Conclusions

The study yields the influence of silver particles on titanate nanotubes and effect of thermal treatment on the morphology. It was found that the silver loaded product, which was initially at nanotubular structure before the thermal treatment, completely transforms into nanoparticles upon thermal treatment for 24 hours at 600 ^{o}C as shown in *Fig 10 and Fig 11*. These finding are also incorporated with the studies of other authors [10]. This change is associated with the collapse of layered structure in nanotubes during thermal treatment. The strong interaction between Silver particles in the interlayer structure and the Oxygen presence in the titanate form also plays a role in this collapse and leads to the formation of nanoparticles.

In pre-edge study of XAS spectrum, shifting of position of pre-edge peak was noticed. The peak position depends on the symmetry of crystal and since it was observed that peak position of thermally treated product approaching towards peak position of anatase phase. It means that the nanotubular product before thermal treatment was transformed into anatase phase upon thermal treatment. The study also showed the effect of concentration of silver in the phase transformation because the sample that contained high concentration of silver was more close to anatase phase compared to the samples with low silver concentrations.

It was reported in the previous studies [11, 12] that the anatase TiO_2 lost its octahedral symmetry when it was converted into titanate nanotubes by using suitable temperature for thermal treatment and washing process during hydrothermal synthesis method. In this study it is found that the titanate nanotubular product again acquired the octahedral symmetry and lost the nanotubular structure. The two factors that play role for this transformation are the concentration of Ag metal during metal ion exchanged method and temperature for thermal treatment process.

Acknowledgement

I would like to thank my supervisor Sophie Canton for guidance and support throughout this project. I am also very thankful to her for giving me an opportunity to visit the University of Szeged that enhanced my ability of working in different environment.

I would also like to thank Akos, Bandi and Laci the faculty members of Department of chemical and environmental Sciences, University of Szeged, for their help to perform the synthesis and initial analysis.

Last but not least, I would like to thank my parents because without their prayers and support I wouldn't be able to do this.

Thanks to all.

Lund, December 18, 2011.

References:

[1] T. Kasuga, M. Hiramatsu, A. Hoson, T. Sekino, K. Niihara. 1998. Formation of Titanium Oxide Nanotube. Langmuir 14: 3160-3163.

[2] Y. C. Nah, I. Paramasivam, P. Schmuki. 2010. Doped TiO_2 and TiO_2 Nanotubes: Synthesis and Applications. ChemPhysChem 11:2698-2713.

[3] D. Gong, C. A. Grimes, O. K. Varghese, W. Hu, R. S. Singh, Z. Chen, E. C. Dickey. 2001. Titanium oxide nanotube arrays prepared by anodic oxidation. J. Mater. Res., Volume 16, Number 12: 3331- 3334.

[4] S. A. Cynthia. 2011. Master Thesis Tuning of Ag/TiONW nanocomposites for antibacterial applications. University of Szeged.

[5] Titanate and Titania Nanotubes. Synthesis, Properties and Applications by D. V. Bavykin and F. C. Walsh.

[6] F. Jalilehvand. 2000. Doctoral Thesis Structure of Hydrated Ions and Cyanide Complexes by X-ray Absorption Spectroscopy. Royal Institute of Technology.

[7] http://www.maxlab.lu.se/beamlines/bli811/.

[8] http://en.wikipedia.org/wiki/Wiggler_(synchrotron).

[9] *D. E. Sayers, E. A. Stern, F. W. Lytle. 1971. New technique for Investigating Noncrystalline structures: Fourier Analysis of the extended X-ray-Absorption Fine structure. Physical Review Letters Volume 27, Number 18: 1204-1207

[10] F.Cesano, S. Bertarione, M.J. Uddin, G. Agostini, D. Scarano, A. Zecchina. 2010. Designing TiO2 based nanostructures by control of surface morphology of pure and silver loaded titanate nanotubes. J. phys. Chem. C. Volume 114: 169-178.

[11] T. Kubo, A. Nakahira. 2008. Local Structure of TiO_2 –Derived Nabotubes prepared by the Hydrothermal Process. J. Phys. Chem. C, Volume 112, Number 5: 1658-1662.

[12] Zoran V. Saponjic, Dimitrijevic, D. M. tiede, A. J. Goshe, X. Zuo, Lin X. Chen, Amanda S. Barnard, Peter Zapol, L. Curtiss, T. Rajh. 2005. Shaping Nanometer-Scale Architecture Through Surface Chemistry. Adv. Mater. Volume 17, Number 8: 965- 971.

[13] D. E. Sayers, E. A. Stern. 1975. New Methods to measure structural disorders. Physical Review letters Volume 35, Number 9: 584-587.

[14] E. Horvath, A. Kukovecz, Z. Konya, I. Kiricsi. 2007. Hydrothermal Conversion of Self-Assembled Titanate Nanotubes into Nanowires in a revolving autoclave. Chem. Mater. 19: 927-931.

[15] M. Y. Guo, M. K. Fung, F. Fang, X. Y. Chen, A. M. C. Ng, A.B. Djurisic, W. K. Chan. 2011. ZnO and TiO_2 1D nanostructures for photocatalytic applications. Journal of Alloys and compounds 509: 1328-1332.

[16] X. Sun, Y. Li. 2003. Synthesis and characterization of Ion-exchange Titanate Nanotubes. Chem. Eur. J. 9: 229-2238.

[17] J. G. Zhou, H. T. Fang, J. M. Maley, M. W. Murphy, J. Y. Peter, J. N. Cutler, R. Sammynaiken, T. K. Sham, M. Liu, F. Li. 2009. Electronic Structure of TiO_2 nanotubes arrays from X-ray absorption near edge structure studies. J. Mater. Chem 19: 6804-6809.

[18] A. Kukovecz, M. Hodos, Z. Konya, I. Kiricsi. 2005. Complex-assisted one-step synthesis of ion-exchangeable titanate nanotubes decorated with CdS nanoparticles. Chemical Physics Letters 411: 445-449.

[19] V. Lucca. 2009. Comparision of Size-Dependent Stuctural and Electronic Properties of Anatase and Rutile Nanoparticles. J. Phys. Chem. C 113: 6367-6380.

[20] A. Kukovecz, M. Hodos, E. Horvath, G. Radnoczi, Z. Konya, I. Kiricsi. 2005. Oriented Crystal Growth Model Explains the Formation of Titania Nanotubes. J. Phys. Chem. B, Volume 109, Number 38: 17781-17783.

[21] G. Mogilevsky, Q. Chen, H. Kulkarni, A. Kleinhammes, W. M. Mullins, Y. Wu. 2008. Layered Nanostructures of Delaminated Anatase: Nanosheets and Nanotubes. J. Phys. Chem. C 112: 3239-3246.

[22] M. T. Byrne, J. E. McCarthy, M. Bent, R. Blake, Y. K. Gun'ko, E. Horvath, Z. konya, A. Kukovecz,I. Kiricsi, J. N. Coleman. 2007. Chemical functionalisation of titania nanotubes and their utilization for the fabrication of reinforced polystyrene composite. Journal of Materials Chemistry 17: 2351-2358.

[23] K. Fukuda, I. Nakai, C. Oishi, M. Nomura, M. Harda, Y. Ebina, T. Sasaki. 2004. Nanoarchitecture of Semiconductor Titania Nanosheets Revealed by Polarization –Dependent Total Reflection Fluorescence X-ray Absoption Fine structure. J. Phys. Chem. B 108: 13088-13092.

[24] V. J. Rose, B. Poumellec. 1999. Coordination octahedron distortion effect on X-ray absorption fine structures of titanium in the rutile titanium dioxide. J. Phys. : Condens. Matter 11: 1123-1137.

[25] D.V.Bavykin, J. M. Friedrich, F. C. Walsh. 2006. Protonated Titanates and TiO_2 Nanostructured Materials: Synthesis, Properties and Applications. Advance Material 18:2807-2824.

[26] T. Kasuga, M. Hiramatsu, A. Hoson, T. Sekino, K. Niihara. 1999. Titania Nanotubes Prepared by Chemical Processing. Advance Material 11, Number 15: 1307-1311.

[27] D. V. Bavykin, F. C. Walsh. 2009. Elongated Titanate Nanostructurs and their Applications. Eur. J. Inorg. Chem: 977-997.

[28] C. A. Grimes. 2007. Synthesis and application of highly ordered arrays of TiO_2 nanotubes. Journal of Material Chemistry 17: 1451- 1457.

[29] Francois Farges, G. E. Brown Jr., J. J. Rehr. 1996. Coordination chemistry of Ti (IV) in silicate glasses and melts: I. XAFS study of titanium coordination in oxide model compounds.

[30] T.M. Grehk and P.O. Nilsson,The Design of the Material Science Beamline, I811, at MAX II, Nucl. Instr. and Meth. in Phys. Res. A 467-468, 635, 2001.